

Original Paper

Plasma cell tumour progression in iMyc^{E μ} gene-insertion mice

JS Kim,^{1†‡} SS Han,^{1‡} SS Park,^{1†} N McNeil² and S Janz^{1*}

¹Laboratory of Genetics, Center for Cancer Research (CCR), National Cancer Institute (NCI), NIH, Bethesda, MD, USA

²Genetics Branch, CCR, NCI, NIH, Bethesda, MD, USA

*Correspondence to:

Dr S Janz, LG, CCR, NCI, Building 37, Room 3140A, Bethesda, MD 20892-4256, USA.

E-mail: sj4s@nih.gov

†Current address: Korea

Research Institute of Bioscience and Biotechnology, Daejeon, South Korea.

‡These authors contributed equally to this paper and should thus be considered first authors.

Abstract

The authors have recently reported that gene-targeted iMyc^{E μ} mice that carry a His₆-tagged mouse *Myc* cDNA, *Myc*^{His}, just 5' of the immunoglobulin heavy-chain enhancer, E μ , are prone to 'spontaneous' neoplasms of the B-lymphocyte lineage. The present study has used histological, immunohistochemical, and molecular genetic methods to investigate a subset of these neoplasms referred to as extraosseous plasmacytomas (PCTs). It is shown that 20.8% (20/96) of tumour-bearing iMyc^{E μ} mice on a mixed genetic background of segregating C57BL/6 and 129/SvJ alleles develop PCT by 500 days. The *Myc*^{His}-induced PCTs produced monoclonal immunoglobulin and developed in the gut-associated lymphoid tissue (GALT), particularly the mesenteric node and Peyer's patches. The PCTs overexpressed *Myc*^{His}, at the expense of normal *Myc*, and exhibited gene expression changes on cDNA macroarrays that were consistent with *Myc*^{His}-driven neoplasia. Surprisingly, in one of three PCT-derived cell lines, *Myc*^{His} was 'replaced' by a naturally occurring T(12;15) translocation, which changed the mode of *Myc* deregulation from gene insertion (*Myc*^{His} transgene) to chromosomal translocation (juxtaposition of normal *Myc* to the immunoglobulin heavy-chain locus *Igh*). These findings provide evidence that recreation of the mouse PCT-associated T(12;15)(*Igh*^{E μ} -*Myc*) translocation by gene insertion in mice results in the predictable development of PCTs in approximately one-fifth of the tumour-bearing mice. *Myc*^{His}-driven PCTs recapitulate aspects of human plasma cell neoplasms, for which relatively few models exist in mice. For example, PCT development in the iMyc^{E μ} mice may provide a good system to study the mechanism by which human *MYC* facilitates the progression of plasma cell myeloma (multiple myeloma) in humans.

Copyright © 2006 Pathological Society of Great Britain and Ireland. Published by John Wiley & Sons, Ltd.

Keywords: mouse models of human plasma cell neoplasms; *Myc*; mouse T(12;15)(*Igh*-*Myc*) translocation; human t(8;14)(q32;q24) translocation

Received: 4 October 2005
Revised: 14 November 2005
Accepted: 28 November 2005

Introduction

Plasmacytomas (PCTs) are malignant neoplasms of terminally differentiated B lymphocytes that occur in many mammalian species including humans and mice. Mouse PCT is of special interest because it provides an experimental model system for the study of the mechanisms by which plasma cell neoplasms, such as extraosseous plasmacytoma and plasma cell myeloma, develop in humans. Since spontaneous PCTs are rare in inbred or wild mice [1], efforts have been made to develop transgenic mice that are genetically prone to these tumours. The first success along this line took advantage of transgenic *v-Abl* expressed in B-lineage cells under the control of the intronic immunoglobulin heavy-chain enhancer E μ [2]. Other approaches utilized transgenes, such as E μ -*Bcl2* [3,4] and E μ -*Bclx* [1], that protect incipient plasma cell tumours from apoptosis. A somewhat surprising development is a mouse model in which PCTs occur predictably because

of transgenic expression of the *NPM-ALK* fusion gene [5,6], the hallmark mutation of the human T-cell lymphoma, anaplastic large cell lymphoma [7]. Additional work is warranted to sort out the strengths and limitations of the various transgenic mouse models and translate the insights gleaned from individual models into tangible benefits for patients with plasma cell neoplasms.

We have recently reported that BALB/c mice that carry a widely expressed human *IL6* transgene driven by the H2-L^d promoter develop PCTs with high incidence [8]. The tumours arise predominantly in the gut-associated lymphoid tissue (GALT), particularly the mesenteric node and Peyer's patches, and contain in most [8], but not all, cases [9] a chromosomal T(12;15) translocation that results in the deregulation of *Myc* (*c-myc*) due to juxtaposition to enhancers in the immunoglobulin heavy-chain locus *Igh*. In a related study, we used gene targeting in mice to recapitulate the fine structure of the T(12;15) translocation found

in approximately 20% of *IL6*-transgenic GALT PCTs: the head-to-head juxtaposition of *Myc* and the intronic *Igh* enhancer, $E\mu$ [10]. The gene-targeted mice, designated $iMyc^{E\mu}$, contain a His₆-tagged mouse *Myc* cDNA, Myc^{His} , inserted head-to-head just 5' of $E\mu$. In addition to the mouse PCT T(12;15) translocation, these mice mimic the human t(8;14)(q24;q32) translocation that juxtaposes $E\mu$ and *MYC* in the human post-germinal centre B-cell tumour, endemic Burkitt lymphoma [11]. Recent results indicate that $iMyc^{E\mu}$ mice on a mixed genetic background of segregating C57BL/6 and 129/SvJ alleles are prone to mature B-cell neoplasms, including IgM⁺ lymphoblastic B-cell lymphomas with Burkitt-like morphology (~50% of all tumours), Bcl-6⁺ diffuse large B-cell lymphoma (~20%), and, interestingly, PCTs (~20%) [10].

Here we describe in greater depth the morphological and molecular features of the PCTs that developed in the $iMyc^{E\mu}$ mice. We show that these tumours exhibit close histogenetic and morphological resemblance to 'spontaneous' GALT PCTs in *IL6*-transgenic BALB/c mice [8]. Our findings extend the body of currently available transgenic mouse models of 'spontaneous' plasma cell tumours by a *Myc*-driven one. Considering that human *MYC* appears to be an important tumour progressor gene in multiple myeloma, the $iMyc^{E\mu}$ model system may provide a good tool to study the mechanisms by which *MYC* drives myeloma progression in humans.

Materials and methods

Mice, tumour diagnosis, and establishment of PCT cell lines

The $iMyc^{E\mu}$ mice were developed by inserting a histidine-tagged mouse *Myc* cDNA into *Igh* just 5' of the intronic heavy-chain enhancer, $E\mu$. Incipient PCTs were detected by monitoring mice for enlarged abdominal lymph nodes and splenomegaly. Mice were bred and maintained on the NIH campus and fed Purina Mouse Chow 5001 *ad libitum* and sterilized, acidified drinking water. The study was conducted under NCI Animal Study Protocol LG-028. Cell lines were established by preparing single-cell suspensions from tumours that were transferred *in vitro* in the presence of IL-6.

Histology and immunohistochemistry

Sections (4 μ m) of paraffin-embedded tissues were stained with H&E, Giemsa, PAS, or methylgreen pyronine. Tissues were classified as exhibiting plasma cell abnormalities including plasmacytosis (accumulations of normal-appearing, non-dividing plasma cells), plasma cell hyperplasia (PCH; mixtures of normal and aberrant hyperchromatic, sometimes mitotically active plasma cells), incipient PCT (isolated clusters or nodules of malignant plasma cells), and overt PCT. Avidin-biotin immunoperoxidase techniques

with antisera to L and H chains (Southern Biotechnology Associates), B220 (CD45R) (CalTag), CD19, and CD138 (syndecan) (Pharmingen) were employed for the determination of Ig production and surface marker expression as previously described [12].

V(D)J rearrangements

For Southern hybridization of clonotypic V(D)J rearrangements, genomic DNA obtained from tumour tissues was digested with EcoRI (*Igh*) or EcoRI and BamHI (*Igk*), fractionated by electrophoresis on 0.7% agarose gels, transferred onto a nitrocellulose membrane, and hybridized to a ³²P-dCTP labelled 1.5 kb HindIII/EcoRI *Igh* probe (pJ11) spanning J_H3 and $E\mu$ or a 1.1 kb $C\kappa$ probe. The latter probe was generated by PCR using a primer pair (forward: 5'-GAT GCT GCA CCA ACT GTA TCC A; reverse: 5'-GGG GTG ATC AGC TCT CAG CTT) developed by Dr M Kuehl (NCI, NIH).

Paraproteins

Serum paraproteins were detected with the Paragon SPE electrophoresis kit (Beckman-Coulter). Ig isotypes were determined by ELISA using Immulon II plates (Dynex Technologies) and isotype-specific goat anti-mouse serum labelled with horseradish peroxidase (Southern Biotechnology). Mouse serum samples were diluted from 10⁻³ to 1.28 × 10⁻⁵. Plates were read on a Molecular Dynamics microplate reader at 450 nm.

Allele-specific RT-PCR of *Myc* and Myc^{His} mRNA

For semi-quantitative determination of *Myc* and Myc^{His} mRNA, total RNA was isolated using TRIzol (Sigma, St Louis, MO, USA). The integrity of RNA was verified by electrophoresis. Double-stranded cDNA was synthesized from 1 μ g of total RNA, using the AMV Reverse Transcriptase kit (Roche, Indianapolis, IN, USA). A common 5' primer for both Myc^{His} and *Myc* (5'-TCT CCA CTC ACC AGC ACA AC-3') was combined with a specific 3' primer for Myc^{His} (5'-CCT CGA GTT AGG TCA GTT TA-3') and *Myc* (5'-ATG GTG ATG GTG ATG ATG AC-3') to distinguish the two messages. Thermal cycling conditions were as follows: 95 °C for 5 min (initial template denaturation), followed by 20 cycles of amplification at 57 °C (primer annealing), 72 °C (extension), and 95 °C (melting), each for 1 min. PCR amplification of *Aktb* cDNA was performed for each sample as a control using the following primer pair: 5'-GCA TTG TTA CCA ACT GGG AC-3' (forward) and 5'-AGG CAG CTC ATA GCT CTT CT-3' (reverse). PCR products were analysed by electrophoresis in 1% agarose gel and visualized by staining with ethidium bromide.

Cytogenetic analysis of PCT-derived cell line 8526

Cells were lysed in hypotonic KCl solution and chromosomes were fixed in methanol-acetic acid (3:1).

Myc-induced plasmacytoma in mice

For each tumour, at least ten complete metaphase plates were analysed. The T(12;15)(*Igh-Myc*) translocation was detected by whole chromosome painting and FISH. The painting and BAC probes hybridizing to chromosome 12 and *Igh* or chromosome 15 and *Myc* were labelled by nick translation with biotin or Spectrum Orange, respectively. The biotin was subsequently detected using FITC-conjugated avidin. Images were acquired with a Leica DMRHC epifluorescence microscope equipped with a Sensys CCD camera (Roper Scientific).

Gene expression analysis on cDNA macroarrays

The relative mRNA expression of NF κ B pathway genes was analysed with mouse GEArray™ Q series kits purchased from SuperArray (Bethesda, MD, USA) according to the manufacturer's protocol. Five micrograms of total RNA was prepared using the TriReagent (Sigma) and reverse-transcribed into cDNA using MMLV reverse transcriptase (Promega) and ³²P-dCTP (PerkinElmer Life Sciences, New England Nuclear) as radioactive label. The labelled cDNA probes were hybridized to gene-specific cDNA fragments spotted on the gene array membrane. Signals were quantitated with a Storm phosphor imager and normalized to the signal of *Gapd* on the same membrane.

Verification of gene array results using RT-PCR

For semi-quantitative determination of mRNA of selected target genes, total RNA was isolated and cDNA was synthesized as described above. PCR primers and thermal cycling conditions are available upon request. PCR amplification of *Gapd* cDNA was performed for each sample as a control using the following primer pair: 5'-GCA TTG TTA CCA ACT

GGG AC-3' (forward) and 5'-AGG CAG CTC ATA GCT CTT CT-3' (reverse). PCR products were analysed by electrophoresis in 1% agarose gel and visualized by staining with ethidium bromide.

Verification of gene array results using qPCR

Total RNA was isolated from cells and tissues using TRIzol Reagent (Invitrogen).

For quantitative Taqman RT-PCR, serial dilutions of input RNA (100 ng–1.56 ng) were analysed in triplicate using the ABI PRISM 7900HT sequence detector system, primers, probes, and the Taqman One-Step RT-PCR Master Mix Reagents kit, all purchased from Applied Biosystems. The reaction mixture was held at 48 °C for 30 min for reverse transcription of RNA into cDNA, followed by incubation at 95 °C for 10 min to activate the Taq polymerase. PCR amplification of cDNA was performed for 40 cycles using the following cycling conditions: denaturing for 15 s at 95 °C and annealing and extending for 1 min at 60 °C. All samples were tested in triplicate and average values were used for quantification. Analysis was performed using SDS v2.1 software (Applied Biosystems) according to the manufacturer's instructions. *Aktb*, which encodes cytoplasmic β -actin, was used as an internal reference gene. The comparative CT method ($\Delta\Delta$ CT) was used for quantification of gene expression.

Results

Incidence, onset, and histological subtypes of PCTs

The incidence of PCT was determined in *iMyc*^{E μ} mice (Figure 1A, bottom) on a mixed genetic background of segregating C57BL/6 and 129/SvJ alleles

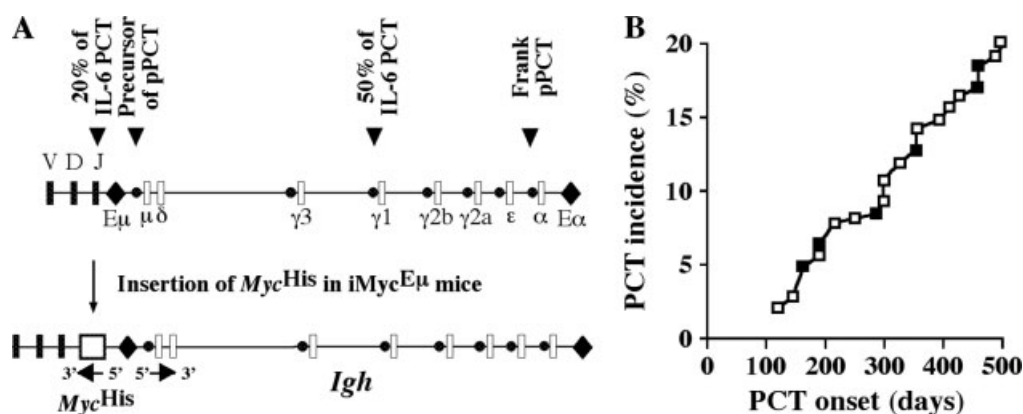


Figure 1. Generation of *iMyc*^{E μ} mice and PCT onset and incidence in these mice. (A) Sites of *Igh* chromosome breakage and translocation with *Myc* in mouse PCTs and targeted transgenic insertion of *Myc*^{His} in *iMyc*^{E μ} mice. A scheme of the normal mouse *Igh* locus (top) and the targeted *Igh* locus (bottom) with the inserted *Myc*^{His} (open box) in *iMyc*^{E μ} mice is shown. The transcriptional orientation of *Igh* and *Myc*^{His} is indicated by horizontal arrows. The gene insertion site is also the preferred recombination site in 20% of mouse T(12;15)(*Igh-Myc*) exchanges found in PCTs that developed 'spontaneously' in C.1L6 mice [8]. The corresponding recombination sites in the majority (~50%) of IL6-transgenic mouse PCTs, inflammation-induced peritoneal PCTs (pPCT), and their precursors take place in the switch regions of γ 1, C α , and C μ , respectively. (B) Onset and incidence of PCTs in untreated *iMyc*^{E μ} mice. Fourteen PCTs (open squares) from a previous study involving 76 tumour-bearing mice [10] and six PCTs (closed squares) from the present, ongoing study thus far involving 20 tumour-bearing mice are included. The current incidence of PCT is 20.8% (20 of 96 tumours) when both studies are combined

followed to 500 days of age. PCTs were first seen at 3.5 months and then increased slowly but steadily, reaching an incidence of 20.8% (20/96) by 500 days (Figure 1B). Mean tumour onset was 291 ± 117 days (range 116–489 days).

Histological examination of 15 tumours showed that PCTs occurred as the three distinct subtypes described in the Bethesda proposal of classifying lymphoid tumours in mice [13]. Representative tissue sections are shown in Figure 2. Seven tumours were mature plasmacytic PCTs (medium-sized sIg⁻ cIg⁺ CD138⁺ cells, pyroninophilic cytoplasm, round eccentric nucleus with margined chromatin and one or several nucleoli; Figure 2A); five tumours exhibited less mature, plasmacytoid or plasmablastic features (medium to large-sized plasma cells; less cytoplasm, a more central nucleus, and more prominent nucleoli than plasmacytic PCT; Figure 2B); and three tumours were classified as anaplastic PCT (less than 10% mature plasma cells on a mixed background of immunoblasts, plasmablasts, and intermediate cell forms with large nuclei and a thick nuclear membrane; Figure 2C).

At the time of diagnosis (Figure 1B), all tumours had progressed to an advanced stage characterized by massive enlargement of Peyer's patches and mesenteric lymph node (up to 2 g) and splenomegaly. The enlargement of gut-associated lymph nodes appeared to be the underlying reason for intestinal obstructions or intussusceptions that were occasionally observed in moribund mice. Among the peripheral lymph nodes, the ones in the cervical region were often larger than those draining the extremities. The occurrence of neoplastic plasma cells in blood vessels indicated plasma cell leukaemia (Supplementary Figure 1, see <http://www3.interscience.wiley.com/cgi-bin/jabout/1130/suppmatt.htm>), which led to tumour cell infiltration of all major parenchymatous tissues including liver, kidney, lung, and, as shown in Supplementary Figure 2 (see <http://www3.interscience.wiley.com/cgi-bin/jabout/1130/suppmatt.htm>), haematopoietic bone marrow.

Special findings in PCT-bearing mice

Histological examination of the PCT-bearing iMyc^{E μ} mice included in this study and other iMyc^{E μ} mice not included here revealed special circumstances that are relevant for proper diagnosis of PCT in mice. Two mice that harboured PCT in multiple tissue sites also contained an unclassified tumour in the haematopoietic bone marrow (Figure 3) and a B-cell lymphoma in a lymph node (Supplementary Figure 3, see <http://www3.interscience.wiley.com/cgi-bin/jabout/1130/suppmatt.htm>), respectively. These findings suggested that PCT sometimes develops concomitantly with a second, independent neoplasm.

A different situation was encountered in four mice that harboured B-cell lymphoma with marked plasmablastic and/or plasmacytic differentiation in some

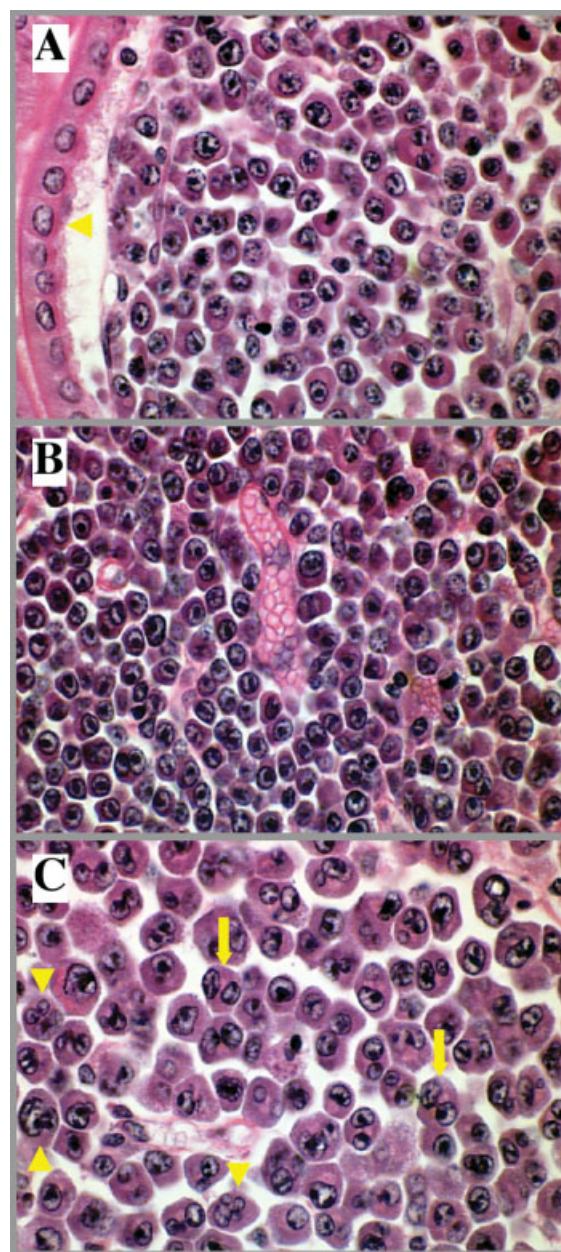


Figure 2. Three types of PCT in iMyc^{E μ} mice: plasmacytic (A), plasmablastic (B), and anaplastic tumours (C). The plasmacytic tumour occurred in a gut villus that is identified by the layer of epithelial cells indicated by a yellow arrowhead. The plasmablastic and anaplastic tumours arose in the GALT. The anaplastic PCT, which corresponds to the moderate end of anaplasia found in these tumours, harbours numerous bi- or multi-nucleated cells (yellow arrows) and irregularly shaped cells containing bizarre nuclei (yellow arrowheads). The three images were taken at the same magnification (40 \times) to facilitate the comparison of tumour types

tissue sites. Since the plasma cells outnumbered the underlying lymphoma cells in these sites (Supplementary Figure 4, see <http://www3.interscience.wiley.com/cgi-bin/jabout/1130/suppmatt.htm>), these cases commanded caution not to be misclassified as PCT.

The third circumstance concerned the tumour stroma. Although PCTs normally contain a diffuse network of Mac2⁺ histiocytes and/or macrophages, the Mac2⁺ cells proliferated focally in some cases,

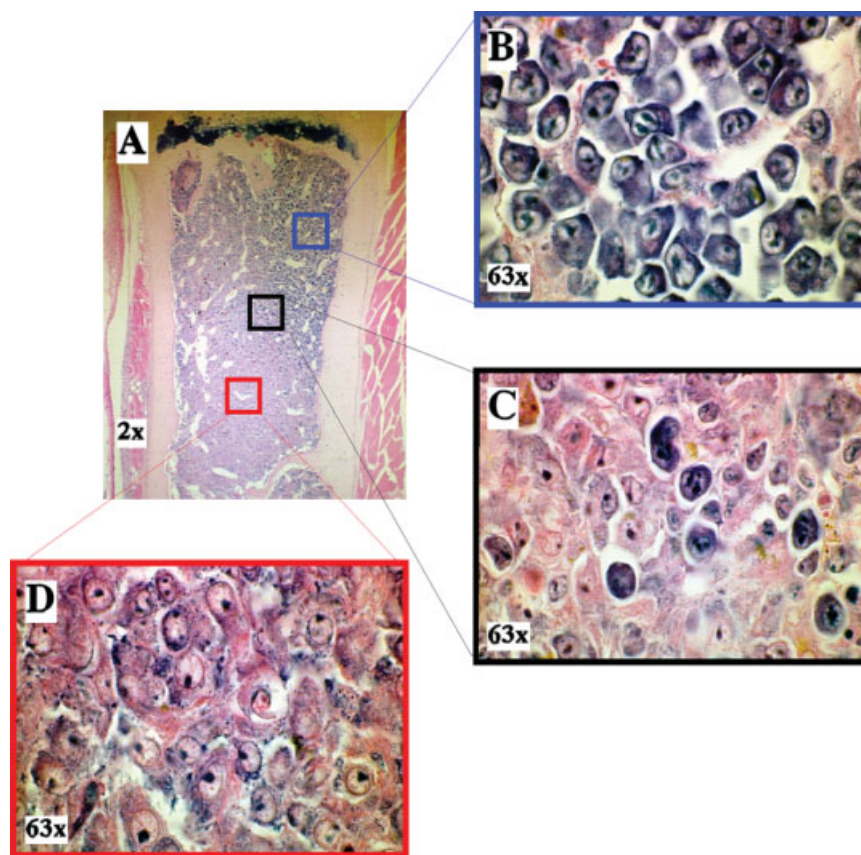


Figure 3. Co-existence of PCT and unknown neoplasm (presumably sarcoma) in the haematopoietic bone marrow of the same mouse. Panel A presents an overview image (Giemsa, 2×) of a histological section of a femur that co-harbours a PCT to the upper right (blue square) and the unclassified tumour in the centre (red square). The borderline zone where PCT and unknown tumour cells intermingle is denoted by a black square. Panels B–D show enlarged views of the three squares included in panel A (Giemsa, 63×). The cytological differences between PCT cells (strongly basophilic cytoplasm, nuclei containing clumped chromatin and usually two or more nucleoli) and presumptive sarcoma cells (metachromatic cytoplasm, vesicular nuclei containing one distinct nucleolus, which is often attached to the nuclear membrane) are clearly apparent

forming cell clusters that could further evolve into polypoid structures (not shown). In three mice, this progressed to bona fide histiocytic sarcoma, which was distinguished by pleomorphic tumour giant cells that contained multiple cell nuclei in a circle or horseshoe-like pattern (Supplementary Figure 5, see <http://www3.interscience.wiley.com/cgi-bin/jabout/1130/suppmatt.htm>). To avoid confusion in the representation of tumour pattern and incidence in *iMyc^{Eμ}* mice, the above-mentioned cases were not included in the PCT incidence curve shown in Figure 1B.

A highly variable feature of PCT-bearing mice was tumour infiltration with T cells. This ranged from essentially absent (not shown) through sparse, diffusely scattered cell infiltrates (Supplementary Figure 6A, see <http://www3.interscience.wiley.com/cgi-bin/jabout/1130/suppmatt.htm>) to highly abundant, dense infiltrates that were seen in three tumours (Supplementary Figures 6B and 6C). These tumours were included in the PCT incidence curve presented in Figure 1B. The significance of these T cells (cytotoxic immune response against the tumour?) is not clear.

These observations underscored that proper PCT classification in *iMyc^{Eμ}* mice requires the investigation

of a representative tissue panel using histological and immunohistochemical methods. The variability of the histopathological findings demonstrated that PCT development is not a uniform process resulting in monomorphic, morphologically indistinguishable tumours. Instead, *Myc^{His}*-induced PCTs presented as distinct subtypes, were accompanied by diverse tissue reactions (eg histiocytes, T cells), and developed sometimes concomitantly with other neoplasms.

Histogenesis of PCT

Because at the time of diagnosis PCTs presented as advanced, disseminated tumours, the tissue site of tumour development remained unknown. To determine this site and evaluate the early stages of PCT development, we sacrificed age-matched, tumour-free mice and then carried out histological examination of a representative tissue panel. Ten groups of mice, each containing three animals, were sacrificed in monthly intervals beginning at 3 months of age. Typical findings are illustrated in Figure 4.

PCTs appeared to originate in many cases in gut-associated lymph nodes, which demonstrated expanded interfollicular and medullary regions due to the

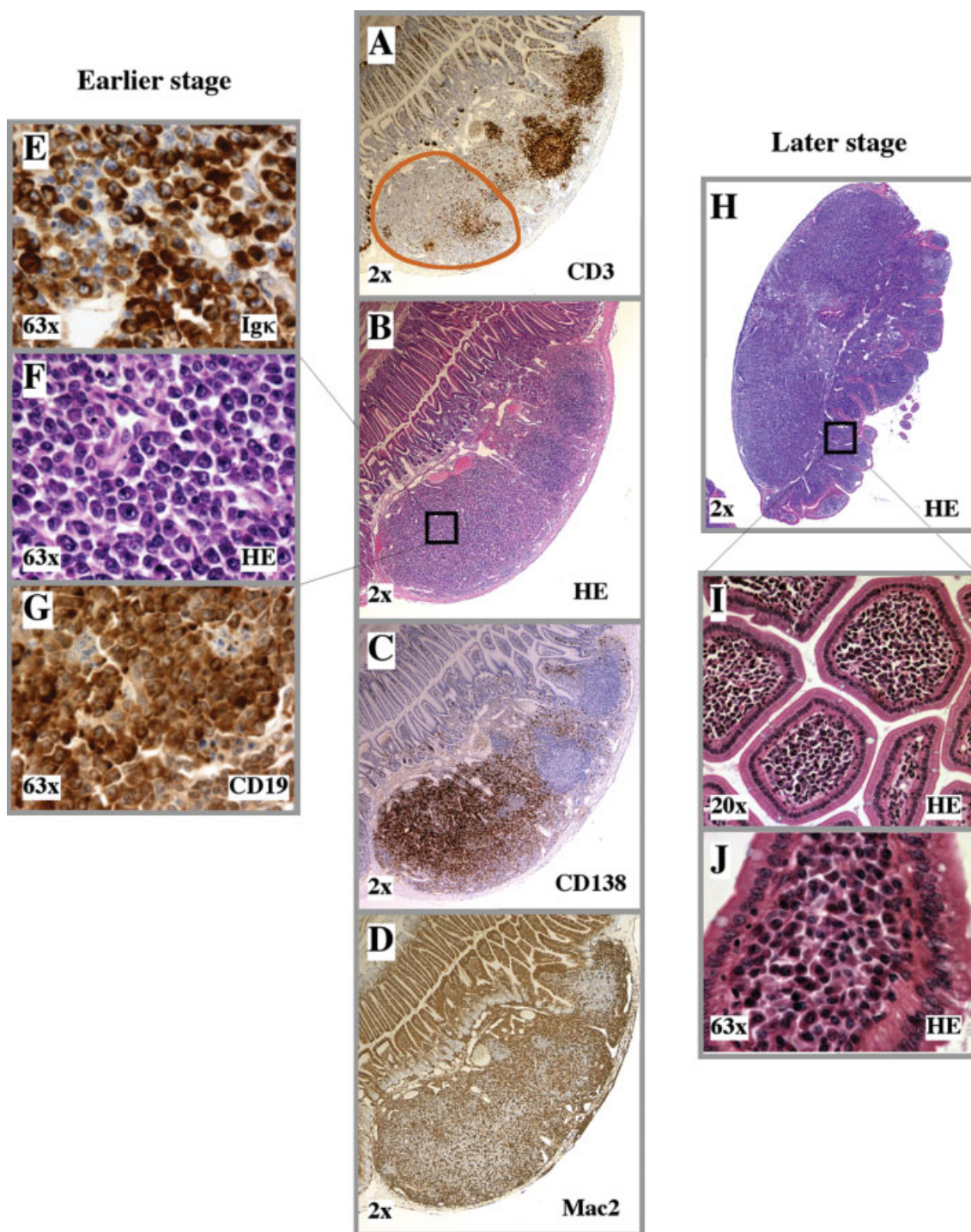


Figure 4. Early stages of PCT development. Panels A–G present a typical incipient PCT that is characterized by the occurrence of a compact nodule of aberrant CD138⁺ plasma cells in the Peyer's patch (circled in panel A). CD3⁺ T cells, which are abundant in the largely normal, upper part of the Peyer's patch, are greatly diminished in the plasma cell nodule (A). A higher-power view of the area indicated by a square in panel B shows that the plasma cells are CD19⁺ (G) and produce κ light-chain (E). Panels H–J present a more advanced stage of tumour development, again using a Peyer's patch as the example. Here, the plasma cell accumulation involves the entire Peyer's patch, and the plasma cells have already invaded the lamina propria of the adjacent gut. This has resulted in thickening of the gut villi, which is illustrated in a transversal section at medium power (I) and a longitudinal section at high power (J)

accumulation of CD138⁺ plasma cells. Focal proliferation of these cells led to nodules, such as the one shown in Figures 4A–4D, which replaced the normal lymph node residents including T cells (panel A) but still contained a normal network of Mac2⁺ cells (panel D). Although most plasma

cells were normal in size and expressed CD19 and immunoglobulin (Figures 4E–4G), closer inspection revealed cytological abnormalities, such as heightened affinity to histological stains (hyperchromasia), increased cell size, and abnormally shaped (cleaved or lobulated) cell nuclei with clumped chromatin. At this

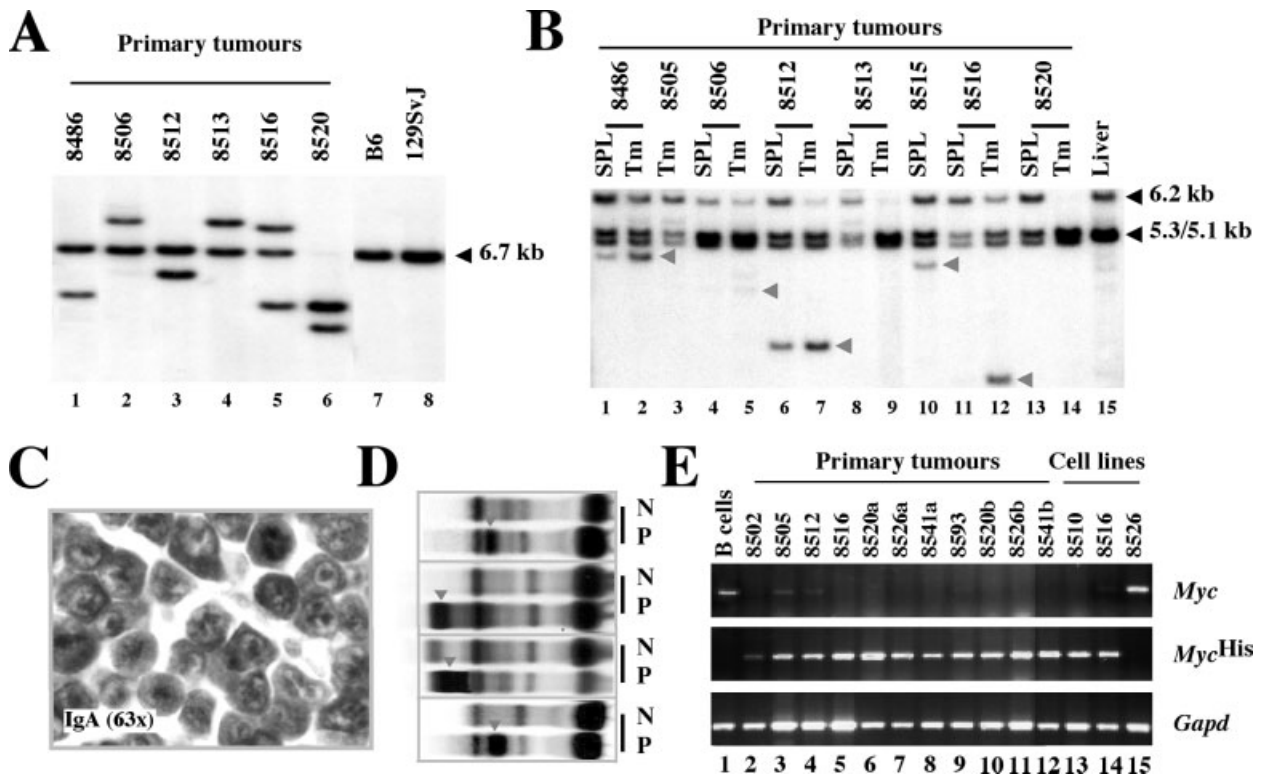


Figure 5. Features of PCT. Southern blots of clonotypic *Igk* (A) and *Igh* (B) rearrangements in primary PCTs are shown at the top. Germ-line fragments are indicated by black arrowheads that are labelled. Liver DNA from inbred C57BL/6 and 129SvJ mice (*Igk* blot, lanes 7 and 8) or *iMyc^{Et}* mice on a mixed C57BL/6 and 129SvJ background (*Igh* blot, lane 15) is included as a control. VJ recombination at the *Igk* locus resulted in clonotypic restriction fragments in six of six PCTs (lanes 1–6). VDJ recombination at the *Igh* locus (grey arrowheads) resulted in clonotypic restriction fragments in five of eight PCTs (lanes 2, 5, 7, 10, and 12) and the loss or reduction of the B6-derived 6.2 kb fragment in two of eight PCTs (lanes 9 and 14). Shown at the bottom are an immunostained section of an *IgA*⁺ PCT, illustrating that tumours with *Igh* rearrangements produce heavy-chain (C); a serum protein electrophoresis gel containing samples from four PCT-bearing *iMyc^{Et}* mice (P) and four normal non-transgenic littermates (N), illustrating that PCTs produce monoclonal Ig (arrowheads pointing down; D); and an RT-PCR agarose gel, indicating the mRNA levels of *Myc* (top), *Myc^{His}* (centre), and *Gapd* (bottom) in normal B cells (lane 1), primary PCTs (lanes 2–12), and PCT-derived cell lines (lanes 13–15; E). Note that all PCT samples except cell line 8526 (lane 15) contained elevated levels of *Myc^{His}*. The 8526 cells (over)expressed normal *Myc* due to a T(12;15) translocation shown in Figure 6

stage, the neoplastic process stayed within the boundary of the lymph node.

The next stage of tumour development was characterized by mucosal invasion of atypical plasma cells that resulted in the infiltration of the lamina propria of gut villi contiguous to Peyer's patches (Figures 4H–4J). Bi- or multi-nucleated plasma cells, some of them containing mitotic figures, were frequent. The continuing proliferation of plasma cells led to incipient PCT, which occurred either as a single, circumscribed, well-demarcated tumour, similar to the nodule shown in Figures 4A–4D, or as scattered clusters of neoplastic plasma cells interwoven in the general plasma cell hyperplasia. The latter was sometimes difficult to detect, because the borderline of plasma cell hyperplasia and incipient PCT is poorly defined using conventional light microscopy.

The diagnosis of PCT was certain when neoplastic plasma cells had migrated to the paracortical and medullary cords of deep and peripheral (particularly cervical) lymph nodes and the red pulp of the spleen. Infiltration of parenchymatous tissues marked the onset of plasma cell leukaemia. There was no clear

association between the age of mice and PCT progression stage; ie severe changes were sometimes found in 3- to 6-month-old mice, while moderate or virtually no changes were seen in 9- to 12-month-old mice.

PCTs are monoclonal tumours that overexpress *Myc^{His}* and produce immunoglobulin

Southern analysis of VJ recombination at the *Igk* locus demonstrated that six of six PCTs had undergone clonotypic gene rearrangements (Figure 5A). VDJ recombination at the *Igh* locus was also readily detectable in seven of eight tumours (Figure 5B), either as tumour-specific restriction fragments (five cases indicated by arrowheads) or as loss of the B6-derived 6.2 kb germline fragment (two cases designated 8513 and 8520). One tumour (8505) did not contain a rearrangement, for reasons that remained unclear. In two of three cases in which tumour and spleen samples were tested side-by-side (8486, 8512, 8516), the same restriction fragments were seen in both tissues (8486, 8512). This showed that the underlying PCT had massively infiltrated the spleen. In all the tumours presented in Figure 4B, the 129-derived *Igh*

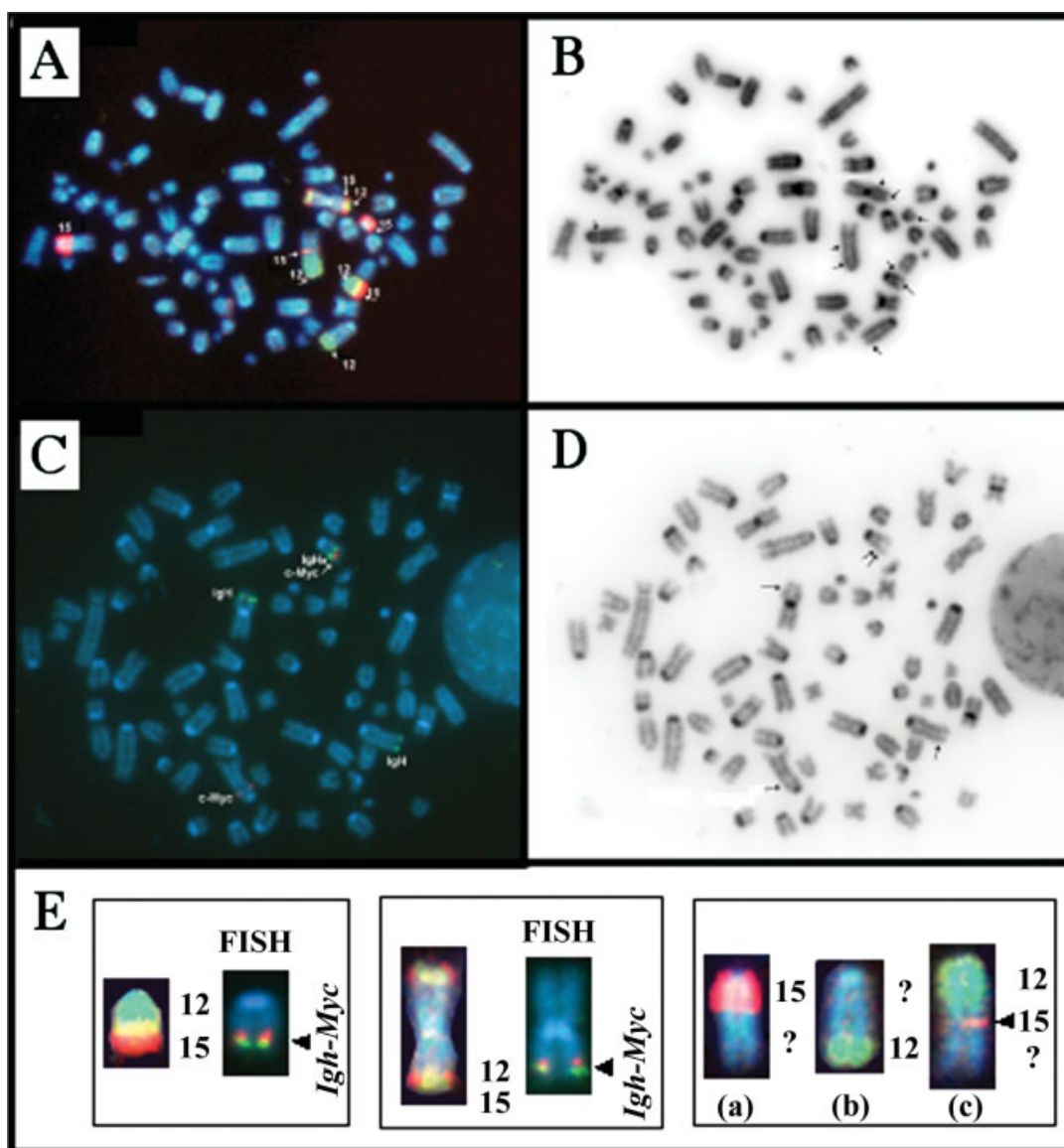


Figure 6. Replacement of Myc^{His} by a T(12;15) translocation in the PCT-derived cell line 8526. A representative metaphase chromosome spread painted with whole chromosome FISH probes for chromosomes 12 and 15 (A) and a computer-generated inverted image of the DAPI counterstain used for chromosome identification (B) are shown at the top. Chromosomes containing 12- or 15-derived material are indicated by arrows. Metaphase chromosomes labelled by gene-specific FISH probes for *Myc* and *Igh* (C) and the inverted DAPI counterstain of the same image (D) are shown in the centre. Chromosomes containing *Myc* and/or *Igh* are indicated by arrows. Various rearrangements of chromosomes 12 and 15 at higher power (E) are shown at the bottom. These include the typical der(12) of a classic, mouse PCT-associated, *Myc*-activating T(12;15)(*Igh*-*Myc*) translocation (left rectangle; yellow indicates the merging of the two painting probes' fluorescent dyes, Spectrum Orange and FITC); a Robertsonian fusion chromosome that contains at the lower telomeric end 12- and 15-derived material, leading to a second *Igh*-*Myc* juxtaposition in the tumour cells (centre rectangle); and, from left to right in the right rectangle, rearrangements of (a) the centromeric portion of 15 with an unknown partner chromosome, (b) the telomeric portion of 12 with an unknown chromosome, and (c) the centromeric portion of 12 with an unknown chromosome that additionally contains a small insert of 15-derived material (arrowhead)

locus that contained the inserted Myc^{His} gene (indicated by the paired 5.3/5.1 kb fragment) remained unaffected by VDJ recombination. This demonstrated that the gene-insertion allele was incapacitated with respect to VDJ recombination, as had been seen in other mice in which the μ heavy-chain gene had been interrupted by gene insertion [14]. The precise mechanism by which Myc^{His} interferes with μ H production remains to be elucidated, but two possibilities are the distortion of germ-line DQ52 and $I\mu$ transcription and the abrogation of V(D)J recombination [15,16].

Immunolabelling of 12 randomly chosen PCTs demonstrated in all cases cytoplasmic heavy-chain (Figure 5C). Consistent with this, the sera of the mice that bore these tumours exhibited M-spikes (paraprotein, monoclonal Ig) that were readily detected by protein electrophoresis using Paragon gels (Figure 5D). Isotyping of these paraproteins using ELISA demonstrated variability in H-chain usage: six were $Ig\gamma$; four were $Ig\alpha$; and two were $Ig\mu$ (not shown). FACS analysis of B-cell and plasma cell markers (results not shown) showed that PCTs were $CD19^+$ $CD3^-$ $Mac2^-$

and either sIg⁻ or dull positive. CD138 (syndecan-1) expression was variable in amplitude but always detectable. B220 expression appeared to be associated with the histological subtype of the tumour: plasmablastic PCTs expressed the surface marker more reliably than the plasmacytic and anaplastic tumours, which had very little or no B220 (not shown).

Allele-specific RT-PCR, which can distinguish *Myc*^{His} mRNA from normal *Myc* mRNA, showed that the transgene was overexpressed compared with the normal *Myc* gene in ten of ten primary tumours (Figure 5E, lanes 2–12) and two of three PCT-derived cell lines (lanes 13–15). This was in agreement with the known negative feedback loop of *Myc* expression [17]. The small amount of normal *Myc* message in two primary tumour samples (lanes 2 and 3) may have been caused by normal cells infiltrating the tumours (eg T lymphocytes), although this was not shown here.

An unexpected observation in one PCT-derived cell line (lane 15) was that normal *Myc* was overexpressed instead of *Myc*^{His}. To elucidate the underlying reason, we performed a number of molecular and cytogenetic studies. The apparent loss of *Myc*^{His} expression in the cell line was readily explained by allele-specific genomic PCR, which demonstrated that *Myc*^{His} was present in the primary tumour from which the cell line was derived (lanes 7 and 11), but deleted in the line (results not shown). Next, we carried out FISH and whole chromosome painting to detect possible rearrangements of normal *Myc* in the cell line (Figure 6). This revealed a complex T(12;15)(*Igh-Myc*) translocation, the primary mechanism of deregulated *Myc* in mouse PCT. These findings showed that in rare circumstances, a *Myc*^{His}-induced PCT may give rise to a cell line in which the transgenic expression of *Myc*^{His} had been replaced with the deregulated expression of normal *Myc* consequent to chromosomal translocation.

Gene expression of PCTs using cDNA macroarrays

Nylon filter membrane cDNA macroarrays provide a useful screening tool to determine the expression of selected 'pathway' genes in mouse plasma cell tumours. To that end, we prepared RNA samples from three primary PCTs. In lieu of normal plasma cells that are difficult to isolate in sufficient numbers from normal mice, we used two RNA samples from MACS-purified C57BL/6 B220⁺ splenocytes as a control. RNA was labelled with ³²P-dUTP and individually hybridized to the cDNA arrays. The individual expression profiles of PCTs were then determined and compared with each other, followed by comparisons with normal mouse B cells.

All RNA samples were evaluated on eight different arrays, each containing 96 genes involved in cell cycle regulation, apoptosis, cancer, signal transduction, stress and toxicity responses, and the NFκB and MAPK pathways. This approach is illustrated in Figure 7A, using the cell cycle array as an example.

The complete data set is presented in Supplementary Figure 7, see <http://www3.interscience.wiley.com/cgi-bin/jabout/1130/suppmatt.htm>. Analysis of the cell cycle array demonstrated that seven genes were up-regulated in PCTs compared with normal B cells (indicated by red squares). Four genes were down-regulated (green squares).

Similar to the cell cycle array, most changes on the other seven arrays were remarkably consistent when PCTs were compared with B cells. Among a total of 768 genes present on the eight gene arrays, 92 (~12%) genes were concordantly up- or down-regulated in PCTs relative to B cells (Figure 7B). A two-fold change in gene expression was used as a threshold. The NFκB array showed the highest number of changes ($n = 24$; one up and 23 down) among the eight arrays, followed by the MAPK ($n = 16$, four up and 12 down), cell cycle and cancer ($n = 11$, three up and eight down) arrays. Altogether, down-regulated genes (67/92, 73%) outnumbered up-regulated genes (25/92, 27%) by a factor of 2.7.

The presence of 21 differentially regulated genes on two or more gene arrays afforded an opportunity to assess further the consistency and reproducibility of the data. Among these genes was *Myc*, which exhibited highly similar levels on five different arrays. Two genes (*Egr1*, *Nfkb1*) were reproducible on four different arrays, three genes (*Atm*, *Nfkb1a*, *Rb1*) on three arrays, and 15 genes (*Birc2*, *Birc5*, *Ccnb2*, *Cnd2*, *Cdkn1b*, *Chek1*, *Ets1*, *Fos*, *Irf1*, *Jun*, *Map2k1*, *Map3k2*, *Odc*, *Tgfb1*, and *Traf1*) on two arrays (Supplementary Table 1, see <http://www3.interscience.wiley.com/cgi-bin/jabout/1130/suppmatt.htm>).

Validation of gene expression using PCR

To validate the above result further, we used semi-quantitative RT-PCR to confirm ten differentially regulated genes that exhibited consistent changes on the gene arrays (Figure 7C). Four up-regulated genes [three from Supplementary Table 1 (*Birc5*, *Ccnb2*, *Myc*) plus *Ccna2*] and six down-regulated genes [five from Supplementary Table 1 (*Egr1*, *Ets1*, *Irf1*, *Map2k1*, *Nfkb1a*) and *Iap1*] were included in the analysis. RT-PCR confirmed the array results for all ten genes. This is illustrated in Figure 7C, which presents corresponding PCR fragments from two primary PCTs (centre and right) next to normal B cells (left), using the housekeeping gene *Gapd*, which was expressed at similar levels in PCTs and B cells, as the control.

To better quantify these results, we performed qPCR in four independent PCT samples and three independent B-cell samples, using commercial kits for all genes included in Figure 7C. The housekeeping gene *Aktb* was used as an internal standard to normalize the data. qPCR confirmed the RT-PCR and array data in all ten cases (Figure 7D). *Myc* was the most highly expressed gene in PCT (12-fold increase relative to B cells), whereas *Egr1* was the most down-regulated gene (ten-fold decrease; see inset with enlarged x -axis

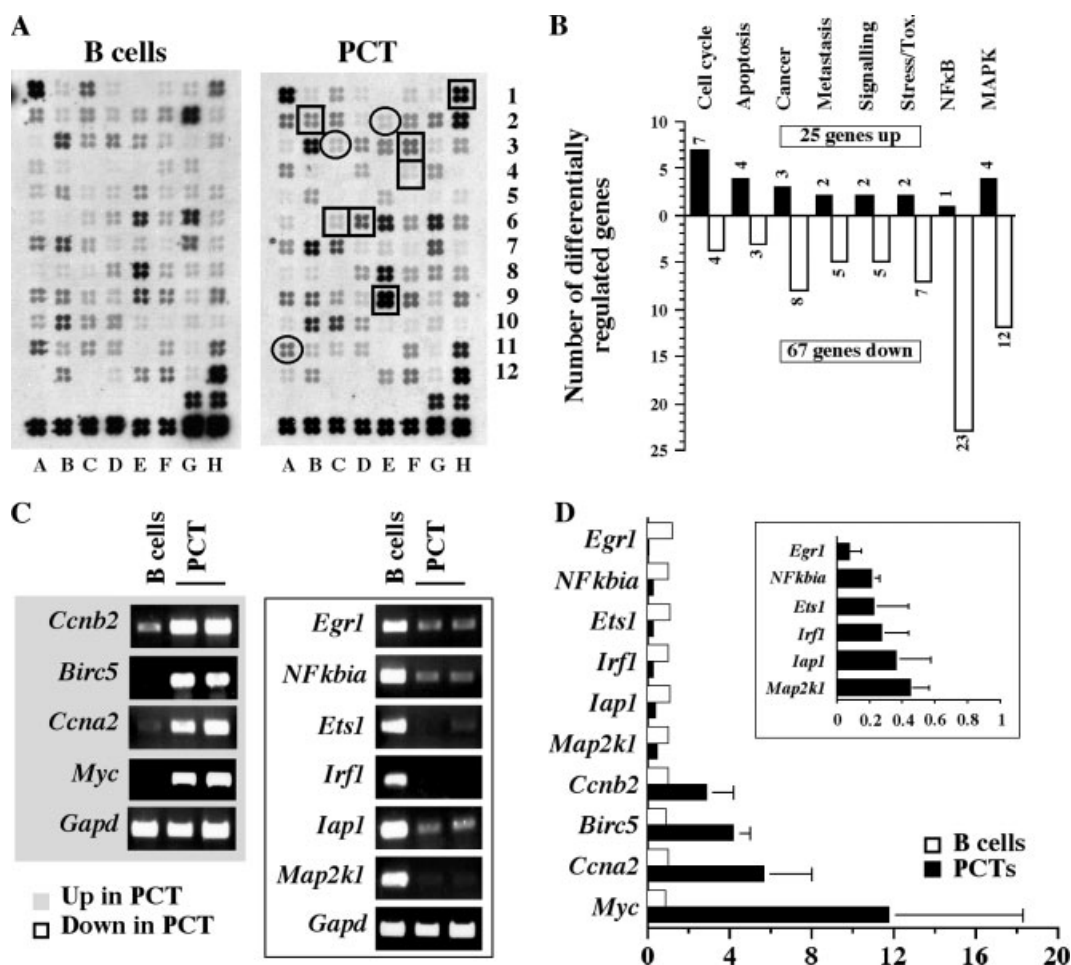


Figure 7. Gene expression in PCTs. (A) Nylon filter membranes containing 96 cell-cycle-related genes (rows 1–12) hybridized to ³²P-labelled RNA samples from a primary PCT (right) and normal C57BL/6 splenocytes (left). Genes that are up- or down-regulated in PCTs compared with normal B cells are indicated by squares and ovals, respectively, on the PCT array. (B) Graphical representation of gene expression changes in PCTs compared with normal B cells using the eight different gene arrays denoted above the columns. The number of genes found to be up- or down-regulated in PCTs is indicated by black and white columns, respectively. (C) Verification of four up-regulated and six down-regulated genes in PCTs compared with normal B cells, using RT-PCR. (D) qPCR analysis of the genes presented in panel C. Mean values and standard deviations based on three independent PCT and B cell samples are shown. The expression values in the B cells were arbitrarily set at 1. The inset uses a smaller scale to show the precise expression levels of the six down-regulated genes in the PCT sample

for better comparison of the six down-regulated genes in PCT).

Consistent with the role of Myc as ‘master’ transcription factor that affects the expression of numerous target genes, eight of the 21 genes listed in Supplementary Table 1 are known Myc targets: *Atm*, *Ccnd2*, *Cdkn1b*, *Jun*, *Myc*, *Odc*, *Rb1*, and *Tgfb1* [18]. Three of these genes are differentially regulated in PCT and normal plasma cells: *Myc* is down-regulated in normal [19] but up-regulated in malignant plasma cells (this study), whereas *Fos* and *Jun* are up-regulated in normal [19] but down-regulated in malignant plasma cells (this study). Additional studies are warranted to evaluate why the positively regulated Myc target, *Ccnd2* (encoding cyclin D2), was down-regulated in PCT.

Discussion

This paper describes a new mouse model of plasma cell tumour development in strain iMyc^{Eμ}. The

Myc^{His}-transgenic PCTs that arose in these mice share many similarities with the tumours that occur in mice that carry a *v-Abl* [2], *Bcl2* [3,4] or *Bclx* [1] transgene under the control of Eμ; a transgenic *NPM-ALK* fusion gene [5,6]; or a human *IL6* transgene driven by an H2 promoter [8]. This band of transgenic PCT models is preceded by the classic model of inflammation-induced peritoneal PCTs in BALB/c mice [20]. It is further complemented by two transplantation-based models that rely either on the *in vivo* propagation of mouse myeloma cell lines of the ‘5T’ series in C57BL/6 mice [21] or on the transfer of human myeloma cells into SCID mice [22]. Each of these mouse models makes a specific contribution to advancing our understanding of neoplastic plasma cell development in human beings, possibly improving therapeutic outcome and leading to new approaches in tumour prevention. Considering that human *MYC* plays an important role in the progression of multiple myeloma [23,24], the iMyc^{Eμ} model system may be

useful for elucidating the mechanism by which *MYC* promotes myelomagenesis in human beings.

The occurrence of PCT in 20% of tumour-bearing iMyc^{E μ} mice provides empirical evidence that our newly developed gene-insertion model of the mouse PCT-associated T(12;15) translocation results in a mode of *Myc* activation that is conducive to malignant plasma cell transformation in mice. More specifically, our findings support the contention that the insertion of *Myc*^{His} in the vicinity of *E μ* results in the accurate recapitulation of the T(12;15) translocation that juxtaposes *E μ* and *Myc* in *IL6*-transgenic GALT PCTs [25]. Additional studies are warranted to elucidate why only one-fifth of the iMyc^{E μ} mice developed PCT (requirement for specific tumour progression events? [10]; present genetic background supports B-cell tumours more strongly than plasma cell tumours?) and why it took on average nearly 10 months (291 days) for these tumours to develop (tempering of *Myc*-dependent cell transformation by *Myc*-dependent apoptosis? [26]).

A few straightforward modifications of the present iMyc^{E μ} mice may further enhance the value of this strain as a model system of neoplastic plasma cell development. Chief among those is the transfer of the *Myc*^{His} transgene to the genetic background of PCT susceptibility, an almost exclusive feature of strain BALB/c [27,28]. The possibility that BALB/c alleles shift the *Myc*^{His}-dependent tumour pattern from B-cell to plasma cell neoplasms is supported by recent evidence that partially backcrossed BALB/c.iMyc^{E μ} mice are hyper-susceptible to inflammation-induced PCT compared with inbred BALB/c mice [29]. As discussed in greater detail elsewhere [26], other modifications of the iMyc^{E μ} mouse may lead to the recapitulation of the bone disease that is seen in human myeloma. There are also approaches for further accelerating PCT development in iMyc^{E μ} mice, such as the expression in these mice of a second transgene that collaborates with *Myc* in plasmacytomagenesis; eg a *Bcl2* family member or *IL6*. Indeed, our most recent data indicate that PCTs arise very rapidly when iMyc^{E μ} is combined with enforced expression of *IL-6* in doubly transgenic *Myc/IL6* mice (SJ, unpublished observation).

In conclusion, this study provides further evidence that the recreation of the T(12;15)(*Igh*^{E μ} -*Myc*) translocation by gene insertion in mice results in the predictable development of PCTs that share key features with PCTs that have acquired this translocation by somatic mutation in individual B or plasma cells. PCT development in iMyc^{E μ} mice may provide a uniquely useful model system for the study of the mechanisms by which human *MYC* drives the progression of plasma cell tumours in human beings.

Supplementary material

Supplementary material may be found at the website <http://www3.interscience.wiley.com/cgi-bin/jabout/1130/suppmatt.htm>

Acknowledgements

We thank the staff of our mouse facility for assistance with the *in vivo* studies; Alexander L Kovalchuk and Seung Tae Chung, NCI, for genotyping and managing our library of tumour samples; Elizabeth B Mushinski, NCI, for immunostaining; Ted A Torrey, NIAID, for FACS analysis; and Thomas Ried, NCI, Herbert C Morse III, NIAID, and Beverly A Mock, NCI, for support. We acknowledge the NCI-CCR Fellow Editorial Board for reading the manuscript and making helpful editorial suggestions. This study was supported by the Intramural Research Program of the NIH, NCI, CCR.

References

1. Potter M. Neoplastic development in plasma cells. *Immunol Rev* 2003;**194**:177–195.
2. Rosenbaum H, Harris AW, Bath ML, McNeill J, Webb E, Adams JM, *et al.* An *E μ -v-abl* transgene elicits plasmacytomas in concert with an activated *myc* gene. *EMBO J* 1990;**9**:897–905.
3. Strasser A, Harris AW, Cory S. *E μ -bcl-2* transgene facilitates spontaneous transformation of early pre-B and immunoglobulin-secreting cells but not T cells. *Oncogene* 1993;**8**:1–9.
4. Silva S, Kovalchuk AL, Kim JS, Klein G, Janz S. BCL2 accelerates inflammation-induced BALB/c plasmacytomas and promotes novel tumors with coexisting T(12;15) and T(6;15) translocations. *Cancer Res* 2003;**63**:8656–8663.
5. Chiarle R, Gong JZ, Guasparri I, Pesci A, Cai J, Liu J, *et al.* NPM-ALK transgenic mice spontaneously develop T-cell lymphomas and plasma cell tumors. *Blood* 2003;**101**:1919–1927.
6. Lange K, Uckert W, Blankenstein T, Nadrowitz R, Bittner C, Renaud JC, *et al.* Overexpression of NPM-ALK induces different types of malignant lymphomas in *IL-9* transgenic mice. *Oncogene* 2003;**22**:517–527.
7. Duyster J, Bai RY, Morris SW. Translocations involving anaplastic lymphoma kinase (ALK). *Oncogene* 2001;**20**:5623–5637.
8. Kovalchuk AL, Kim JS, Park SS, Coleman AE, Ward JM, Morse HC 3rd, *et al.* *IL-6* transgenic mouse model for extraosseous plasmacytoma. *Proc Natl Acad Sci U S A* 2002;**99**:1509–1514.
9. McNeil N, Kim JS, Ried T, Janz S. Extraosseous *IL-6* transgenic mouse plasmacytoma sometimes lacks *Myc*-activating chromosomal translocation. *Genes Chromosomes Cancer* 2005;**43**:137–146.
10. Park SS, Kim JS, Tessarollo L, Owens JD, Peng L, Han SS, *et al.* Insertion of *c-Myc* into *Igh* induces B-cell and plasma-cell neoplasms in mice. *Cancer Res* 2005;**65**:1306–1315.
11. Dalla-Favera R, Bregni M, Erikson J, Patterson D, Gallo RC, Croce CM. Human *c-myc* onc gene is located on the region of chromosome 8 that is translocated in Burkitt lymphoma cells. *Proc Natl Acad Sci U S A* 1982;**79**:7824–7827.
12. Potter M, Mushinski EB, Wax JS, Hartley J, Mock BA. Identification of two genes on chromosome 4 that determine resistance to plasmacytoma induction in mice. *Cancer Res* 1994;**54**:969–975.
13. Morse HC 3rd, Anver MR, Fredrickson TN, Haines DC, Harris AW, Harris NL, *et al.* Bethesda proposals for classification of lymphoid neoplasms in mice. *Blood* 2002;**100**:246–258.
14. Kitamura D, Roes J, Kuhn R, Rajewsky K. A B cell-deficient mouse by targeted disruption of the membrane exon of the immunoglobulin mu chain gene. *Nature* 1991;**350**:423–426.
15. Sakai E, Bottaro A, Davidson L, Sleckman BP, Alt FW. Recombination and transcription of the endogenous Ig heavy chain locus is effected by the Ig heavy chain intronic enhancer core region in the absence of the matrix attachment regions. *Proc Natl Acad Sci U S A* 1999;**96**:1526–1531.
16. Nitschke L, Kestler J, Tallone T, Pelkonen S, Pelkonen J. Deletion of the DQ52 element within the Ig heavy chain locus leads to a selective reduction in VDJ recombination and altered D gene usage. *J Immunol* 2001;**166**:2540–2552.
17. Penn LJ, Brooks MW, Laufer EM, Land H. Negative autoregulation of *c-myc* transcription. *EMBO J* 1990;**9**:1113–1121.

18. Zeller KI, Jegga AG, Aronow BJ, O'Donnell KA, Dang CV. An integrated database of genes responsive to the Myc oncogenic transcription factor: identification of direct genomic targets. *Genome Biol* 2003;**4**:R69.
19. Underhill GH, George D, Bremer EG, Kansas GS. Gene expression profiling reveals a highly specialized genetic program of plasma cells. *Blood* 2003;**101**:4013–4021.
20. Potter M, Boyce C. Induction of plasma cell neoplasms in strain BALB/c mice with mineral oil and mineral oil adjuvants. *Nature* 1962;**193**:1086.
21. Radl J, Croese JW, Zurcher C, Van den Eenden-Vieeven MH, de Leeuw AM. Animal model of human disease. Multiple myeloma. *Am J Pathol* 1988;**132**:593–597.
22. Yaccoby S, Barlogie B, Epstein J. Primary myeloma cells growing in SCID-hu mice: a model for studying the biology and treatment of myeloma and its manifestations. *Blood* 1998;**92**:2908–2913.
23. Shou Y, Martelli ML, Gabrea A, Qi Y, Brents LA, Roschke A, et al. Diverse karyotypic abnormalities of the c-myc locus associated with c-myc dysregulation and tumor progression in multiple myeloma. *Proc Natl Acad Sci U S A* 2000;**97**:228–233.
24. Rasmussen T, Theilgaard-Monch K, Hudlebusch HR, Lodahl M, Johnsen HE, Dahl IM. Occurrence of dysregulated oncogenes in primary plasma cells representing consecutive stages of myeloma pathogenesis: indications for different disease entities. *Br J Haematol* 2003;**123**:253–262.
25. Smith AJ, De Sousa MA, Kwabi-Addo B, Heppell-Parton A, Impey H, Rabbitts P. A site-directed chromosomal translocation induced in embryonic stem cells by Cre-loxP recombination. *Nature Genet* 1995;**9**:376–385.
26. Cheung WC, Kim JS, Linden M, Peng L, Van Ness B, Polakiewicz RD, et al. Novel targeted deregulation of c-Myc cooperates with Bcl-X(L) to cause plasma cell neoplasms in mice. *J Clin Invest* 2004;**113**:1763–1773.
27. Zhang S, Ramsay ES, Mock BA. Cdkn2a, the cyclin-dependent kinase inhibitor encoding p16INK4a and p19ARF, is a candidate for the plasmacytoma susceptibility locus, Pctr1. *Proc Natl Acad Sci U S A* 1998;**95**:2429–2434.
28. Bliskovsky V, Ramsay ES, Scott J, DuBois W, Shi W, Zhang S, et al. Frap, FKBP12 rapamycin-associated protein, is a candidate gene for the plasmacytoma resistance locus Pctr2 and can act as a tumor suppressor gene. *Proc Natl Acad Sci U S A* 2003;**100**:14982–14987.
29. Park SS, Shaffer AL, Kim JS, duBois W, Potter M, Staudt LM, et al. Insertion of Myc into Igh accelerates peritoneal plasmacytomas in mice. *Cancer Res* 2005;**65**:7644–7652.